# High-Pressure Dynamic Light Scattering of Poly(ethylene-*co*-1-butene) in Ethane, Propane, Butane, and Pentane at 130 °C and Kilobar Pressures

**Thomas W. Kermis,[†,#] Dan Li,[‡] Ozge Guney-Altay,[‡] Il-Hyun Park,[§] John H. van Zanten,[⊥,*] and Mark A. McHugh[*,‡]**

*Department of Chemical Engineering, Johns Hopkins University, Baltimore, Maryland 21218; Department of Chemical Engineering, Virginia Commonwealth University, Richmond, Virginia 23284; Department of Polymer Science & Engineering, Kumoh National University of Technology, Kyungbuk, Korea; and Chemical Engineering Department, North Carolina State University, Box 7905, Raleigh, North Carolina 27695-7905*

*Received June 28, 2004; Revised Manuscript Received September 3, 2004*

ABSTRACT: Poly(ethylene-*co*-1-butene) diffusion in ethane, propane, butane, and pentane indicates that ethane solutions are remarkably different. For propane, butane, and pentane the dynamic second virial coefficient, $k_D$, is negative near the phase boundary, increases rapidly to positive values within ~100 to 200 bar of the respective phase boundary, and approaches a constant value at high pressures. For ethane, $k_D$ is also negative near the phase boundary; it increases at a slower rate and becomes only slightly greater than zero. $k_D$ for all four solvents superpose when plotted against "methyl" molar density, suggesting thermodynamic interactions rather than hydrodynamic forces dominate. For propane, butane, and pentane the hydrodynamic radius, $R_H$, also starts at a low value near the phase boundary and increases to the same value for all three alkanes. For ethane $R_H$ is ~30% smaller than those for the higher alkanes, reflecting the poor quality of ethane even 1000 bar above the phase boundary.

## Introduction

Although numerous researchers have used dynamic light scattering (DLS) to study the effect of solvent quality on polymer conformational behavior, these studies are invariably performed with incompressible liquid solvents. Chu,[1−6] Cummins,[7] and Pecora[8,9] pioneered the application of DLS to the study of polymer conformational behavior as solvent quality is varied with multiple liquid solvents or changes in temperature. In contrast, the focus of the present study is to investigate the change in polymer conformational behavior as solvent quality is adjusted via changes in pressure, which requires a reliable high-pressure scattering cell. Several researchers have developed "homemade" high-pressure scattering cells that incorporate a thick sapphire tube[10−12] to hold the polymer solution. The advantages of this cell design are that it fits in a commercially available light scattering instrument, it allows a continuous range of angles to be studied, and it can operate to pressures of 1000 bar.[11] The birefringence of sapphire, however, leads to polarization scrambling of light if the incident beam is not coincident with the optical axis of the sapphire crystal. In addition, sapphire tubes under pressure are subject to radial stress that makes the tube less reliable than flat sapphire windows which have an optical axis coincident with the strength *c*-axis. Hence, several other research groups have developed cells with flat sapphire windows mounted at fixed angles in a high-pressure steel body.[13−19] Although very high pressures can be obtained with this type of cell, careful design is required to minimize the weight of the cell and to maximize the number of detection windows. Compact cells have also been designed with a single, fixed-angle detection window that makes it possible to retrofit the cell to a commercial DLS instrument, and one group has operated such an apparatus to 8000 bar.[13,20−22] Chu and co-workers have designed a compact, fiber-optic, scattering cell capable of operating to 552 bar, although this cell is limited to modest temperatures.[23,24] Nevertheless, this compact cell has yielded information on the pressure effect on the association of diblock copolymers in $CO_2$ and micelle-to-unimer transitions.

Lechner and co-workers have reported high-pressure light scattering studies for polymer−liquid solvent systems that date to the early 1970s.[25−29] In many of their studies they focused on biopolymer−water systems to determine pressure-induced swelling and association/disassociation behavior as a function of pH, temperature to 100 °C, and pressure to 3000 bar.[30] They find that the polymer diffusion coefficient at infinite dilution, $D_0$, increases with increasing temperature but is relatively insensitive to pressure except at high temperatures.[28,29] In addition, $D_0$ can be directly related to the increase of solvent viscosity with pressure, which suggests that polymer−liquid solvent systems at high pressure are reasonably well understood, except perhaps for biopolymer systems. In certain studies, Lechner and co-workers[31] adjust solvent quality using mixed solvents, although these studies are more difficult to interpret unambiguously since one of the solvents can be preferentially associated with the polymer. In contrast, the study presented here uses neat supercritical fluid (SCF) solvents whose quality can be easily varied with changes in the system pressure.

In the early 1970s, Gaeckle and Patterson performed static light scattering studies with solutions of polyisobutylene (PIB) in 2-methylbutane at 24, 57, and 64

[†] Johns Hopkins University.
[‡] Virginia Commonwealth University.
[§] Kumoh National University of Technology.
[⊥] North Carolina State University.
[#] Now at Mead-Westvaco Corporation, Laurel, MD.
* Corresponding authors: e-mail mmchugh@vcu.edu; john_vz@ncsu.edu.

10.1021/ma0487103 CCC: $27.50 
Published on Web 10/29/2004

**Table 1. Physical Property Information on the Normal Alkanes Used in This Study[36,37]**

| | critical temp (°C) | critical press. (bar) | polarizability (Å$^3$) |
|---|---|---|---|
| ethane | 32.2 | 48.8 | 4.4 |
| propane | 96.6 | 42.5 | 6.3 |
| butane | 152.0 | 38.0 | 8.1 |
| pentane | 196.5 | 33.7 | 10.0 |

°C and polystyrene (PS) in 2-butanone at 22 °C. They showed that pressure has a strong effect on polymer−solvent interactions which results in a ∼10% increase in the radius of gyration, $R_g$, for the PIB−2-methylbutane solution and a ∼5% increase in the $R_g$ for the PS−butanone solution.[10] The second osmotic virial coefficient, $A_2$, also increases from small negative value at pressure less than 50 bar to a small positive value at pressure from 50 to 110 bar for the PIB−2-methylbutane solution at 57 and 64 °C.[10] $A_2$ does not increase significantly at 24 °C for the PIB−2-methylbutane system or at 22 °C for the PS−2-butanone system. Although this particular study only went to 110 bar, the authors argue that the increase in $R_g$ and $A_2$ are a result of solvent packing which affects the population of conformations or rotational isomers of the polymer. It is a bit surprising that packing effects would occur with liquid solutions at such modest temperatures and moderate pressures far from the solvent critical point since solvent density only increases by ∼8% over this range of operating conditions.

To the best of our knowledge, van Hook and co-workers are the first group to systematically integrate macroscopic phase behavior studies with microscopic solution structure studies via DLS.[15,16,18,19,32,33] Virtually all of their studies were done with liquid solvents, although many of the studies were performed near liquid−liquid demixing boundaries which is philosophically similar to the approach presented here. van Hook and co-workers have been able to couple the results from DLS and small-angle neutron scattering (SANS) studies to probe the change of inter- and intramolecular correlation lengths over wide ranges of operating variables. In a more recent static light scattering study, van Hook and co-workers show that the effect of pressure on $A_2$ depends on the proximity to the theta point for the polymer−liquid solvent system.[34]

The objective of the present work is to relate the macroscopic phase behavior of poly(ethylene-*co*-20.2 mol % 1-butene) ($PEB_{10}$ with 10 ethane branches per 100 backbone carbon atoms) in ethane, propane, butane, and pentane to the solution microstructure obtained from DLS measurements in the single-phase regions of the binary mixtures. Table 1 shows the critical properties and the polarizabilities of these molecularly simple, nonpolar alkanes which are chosen to facilitate the interpretation of the intermolecular interactions that govern the phase behavior and the response of the polymer chain to its environment. The polarizability, which fixes the magnitude of dispersion interactions, increases with increasing molecular size of the alkane and, therefore, solvent quality also increases with molecular size. The phase behavior and DLS studies reported here are performed with dilute solutions. The DLS study is performed at a single temperature of 130 °C and at pressures close to the phase boundary and increasing to 2100 bar into the single-phase region for each mixture. Hence, the DLS data provide insight into the response of nonpolar $PEB_{10}$ chains to a wide variation in chemical potential environment provided by nonpolar supercritical, near critical, and compressed liquid solvents from the same chemical family. This coupled phase behavior−DLS study complements a previously reported SANS study of $PEB_{10}$ in supercritical ethane and in compressed liquid pentane.[35] Another objective of the present work is to report the characteristics of a multiwindowed (36°, 45°, 72°, 90°, 135°, 144°) scattering cell capable of operating to 2500 bar and temperatures in excess of 150 °C. The high-pressure cell is integrated with a custom-built light scattering apparatus to provide a vehicle to obtain fundamental information at a macromolecular level with exceptionally poor quality SCF solvents and with semicrystalline polymers that require elevated operating temperatures and pressures.

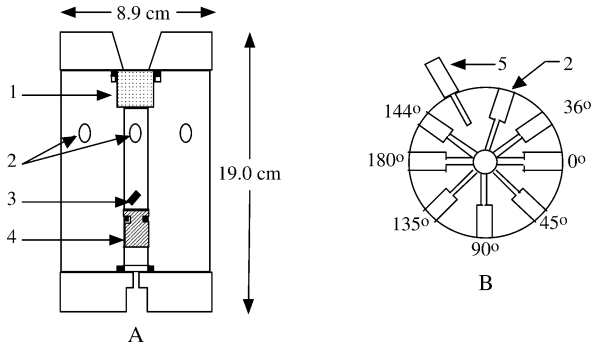


**Figure 1.** Schematic diagram of the high-pressure scattering cell used in these studies: (A) side view; (B) top view; 1, sapphire window sealed with an O-ring and back-up ring; 2, scattering ports at various angles; 3, magnetic stir bar; 4, piston sealed with an O-ring; 5, platinum RTD used for temperature control.

The next section describes the high-pressure DLS apparatus in detail. Experimental DLS data for the polystyrene−toluene system are obtained and compared to previously reported data to verify the reliability of the apparatus and techniques. Then DLS data are reported for $PEB_{10}$ in ethane, propane, butane, and pentane to demonstrate the impact of solvent quality on the response of the $PEB_{10}$ chains on approach to a phase boundary. The results from this DLS study offer insight into the differences between an SCF and a conventional liquid solvent that ultimately can provide a rationale for the application of SCF solvents for polymer processing.

## Experimental Section

Figure 1 is a schematic diagram of the cell developed for DLS measurements of polymer−SCF solutions. The cell is machined from Nitronic 50, a high strength, high nickel content steel that is nonmagnetic so that the contents of the cell can be mixed using a magnet located outside the cell. A sapphire window (1.9 cm o.d. × 1.9 cm thick) fitted into the top of the cell with an unsupported o.d. of 1.3 cm makes it possible to monitor the clarity of the solution and the integrity of the beam to ensure a single-phase exists when operating near a phase boundary. The solution is compressed by displacing a piston using water pressurized with a pressure generator. System pressure is monitored with a transducer/display located on the water side of the piston as it only takes ∼1 bar to move the piston. Solution temperature is maintained to within ±0.3 °C with heating bands and is monitored directly with an internal thermocouple soldered into a cone-and-threaded nipple that fits into a port on the cell. Figure 2 shows a schematic of a custom window holder that seals the window and screws into the cell, making a metal-to-metal seal. Incident light enters through a 0.8 cm o.d. × 1.3 cm thick sapphire

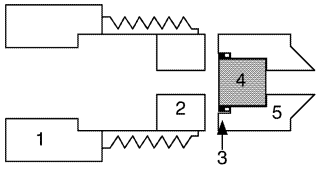


**Figure 2.** Schematic diagram of the window holder: 1, high-pressure gland; 2, window support disk provides a flat surface for seating the window; 3, O-ring and back-up ring for sealing the window; 4, sapphire window; 5, window holder with coned end for pressure seal with the cell body.

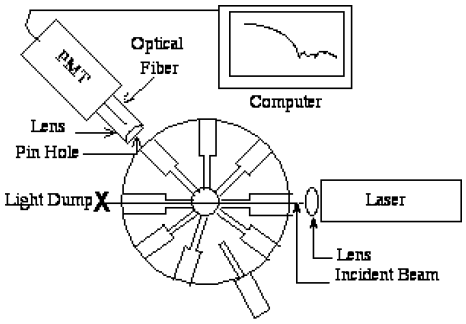


**Figure 3.** Schematic of the high-pressure dynamic light scattering instrument used in the present study.

window with a 0.5 cm unsupported diameter, rated to 21 000 bar. The beam exits into a light dump constructed from tubing bent at 90°, connected to the cell at one end, and capped at the other end to eliminate internal reflections. The smaller detector ports are fit with 0.5 cm o.d. × 0.6 cm thick sapphire windows also rated to 21 000 bar based on the unsupported area.

Figure 3 shows that the DLS cell is concentrically mounted on an adjustable platform at the center of a rotational stage (Newport Corp.), but the cell does not rotate with the stage. The laser (200 mW DPSS Nd:YAG, $\lambda = 532$ nm, Coherent Inc.) is mounted on an adjustable platform and is fitted with a 100 mm EFL plano-convex lens (Newport Corp.) to focus the incident beam at the center of the cell. The detection optics consist of 150 $\mu$m diameter pinhole, followed by a 38.1 mm EFL plano-convex lens that focuses light onto a 150 $\mu$m diameter multimode optical fiber (Wave Optics Inc.). The optical fiber transmits the collected scattered light to an ALV/SO-SIPD/DUAL photomultiplier detector (ALV-Laser) with the fiber collector and photomultiplier detector being mounted on a platform that rotates around the cell. Autocorrelation functions are generated using an ALV-5000 multiple-tau digital correlator that operates in real time with a fixed range of logarithmically spaced lag times between 200 ns and several hours.

Since only half of the detector angles are accessible during each experiment due to geometric constraints of the detector, three of the six ports are fitted with windows, and the other ports of the cell are fitted with a loading valve, an internal thermocouple, and a plug. Scattering experiments are performed once the solution is added to the cell, and the system is equilibrated at the desired pressure and temperature. The detector is rotated to the desired angle and locked into place, and three independent scattering runs are performed at each angle. The duration of each scattering run is determined by the magnitude of the intensity of the scattered light although typically each run lasts 5 min.

The phase behavior for each $PEB_{10}$−alkane mixture is determined using the scattering cell. The phase transitions, or cloud points, are the lowest operating pressure where the solution just begins to appear "hazy", the incident beam exhibits a halo due to multiple scattering, and the scattered light intensity decreases substantially. Propane and butane density data are also determined starting at the respective $PEB_{10}$−alkane phase transition and extending into the single-phase region at high pressures using a previously reported technique.[38−40] Specific experimental details used to measure

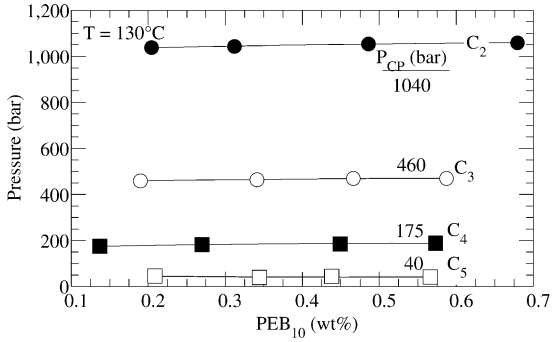


**Figure 4.** Impact of concentration on the phase transition of $PEB_{10}$ in ethane, propane, butane, and pentane at 130 °C. The transition pressure, termed a cloud point, $P_{CP}$, is listed next to each curve.

density are given by Byun et al., who also report that the alkane densities have an accumulated uncertainty of ±1.5%.[40]

**Materials.** The polystyrene (weight-average molecular weight ($M_w$) of 650 000 and a molecular weight polydispersity index ($M_w/M_n$) of 1.06 (Pressure Chemical Co.) was used as received. HPLC grade toluene (Aldrich Co.) was also used without further purification. Four solution concentrations were prepared at room temperature and then stored in clean glass vials. The solutions were loaded into the precleaned scattering cell using a clean glass syringe fitted with a Nalgene 0.2 $\mu$m PTFE membrane filter (Fisher Scientific).

The statistically random poly(ethylene-*co*-20.2 mol % 1-butene) ($PEB_{10}$) was synthesized by Pamela Wright and Lewis Fetters via anionic polymerization of butadiene with subsequent saturation by hydrogenation as described in detail elsewhere.[41−44] The $PEB_{10}$ has an $M_w$ of 232 500, a $M_w/M_n$ of 1.01−1.02, and 10 ethyl branches per 100 backbone carbon atoms. The $PEB_{10}$ sample was stored at 5 °C and used without further purification. The ethane (C.P. grade, 99.1+% purity, Potomac Airgas), propane (scientific grade, 99.95+% purity, MG Industries), *n*-butane (research grade, 99.95% purity, MG Industries), and *n*-pentane (spectrophotometric grade, 99+% purity, Aldrich Chemical Co.) were used without further purification.

## Results and Discussion

**Dilute Solution Phase Behavior.** Figure 4 shows that $PEB_{10}$ concentration has essentially no effect on the location of the phase boundary curves for dilute $PEB_{10}$ concentrations in ethane, propane, butane, and pentane. The compositions shown in Figure 4 are in the concentration range used for DLS measurements. Note that the phase boundary pressure decreases as the polarizability, or molecular size, of the alkane solvent increases. However, the magnitude of the pressure difference between the different solvents also diminishes as the size of the solvent increases. The characteristics of the phase behavior shown in Figure 4 is very similar to that observed for other nonpolar polymer−nonpolar solvent mixtures including polyethylene−alkane mixtures.[45] As expected, supercritical ethane is the weakest solvent while liquid pentane is the strongest solvent. Figure 5 shows the density of each of the alkane solvents starting at their respective $PEB_{10}$−alkane phase boundaries and extending to higher pressures at 130 °C. Details are found elsewhere on the quality of the ethane and pentane density data.[40] The propane and butane density data at pressures less than approximately 700 bar are in good agreement with data reported by Vargaftik[46] for both solvents and by Sen and Kiran for butane.[47] The following equations are used to calculate the density, $\rho$, for each alkane at 130 °C: $\rho_{ethane}$ (g/cm$^3$) $= -0.6685 + 0.11954 \ln(P)$; $\rho_{propane}$ (g/cm$^3$) $= -0.3026$

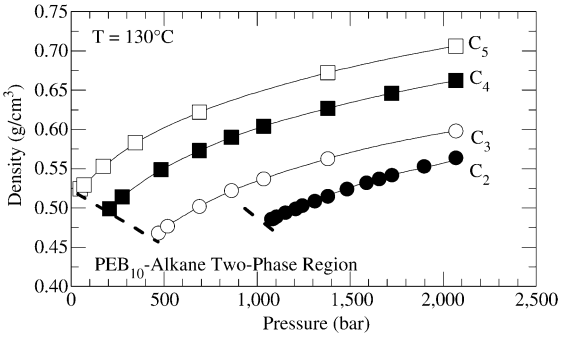


**Figure 5.** Solvent density of ethane,[40] propane (obtained in this study), butane (obtained in this study), and pentane[40] at conditions from the respective $PEB_{10}$−alkane phase boundary, shown with a dashed line, to very high pressures.

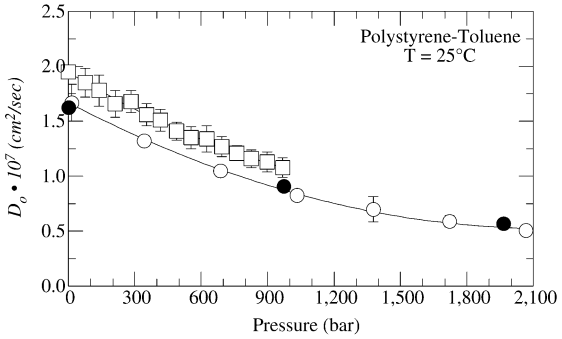


**Figure 6.** Comparison of $D_0$ obtained in the present study (open circles) to data of Freeman[62] (open squares) and to data of Roots and Nystrom[22] (filled circles).

+ 0.08736 ln($P$); $\rho_{butane}$ (g/cm$^3$) = 0.6004 − 0.07781 ln($P$) + 0.00813[ln($P$)]$^2$; $\rho_{pentane}$ (g/cm$^3$) = 0.6438 − 0.07123 ln($P$) + 0.01040[ln($P$)]$^2$ where the pressure is in psia. These density data are subsequently used to analyze the DLS data.

**Dynamic Light Scattering.** For homodyne DLS measurements, the normalized second-order intensity autocorrelation function, $g^{(2)}(q,\tau)$, can be related to the normalized first-order electric field autocorrelation function, $g^{(1)}(q,\tau)$:

$$g^{(2)}(q,\tau) = \beta|g^{(1)}(q,\tau)|^2 + B \quad (1)$$

where $B$ is the baseline, $q$ is the scattering vector defined as $q = |q| = (4\pi n/\lambda_0)\sin(\theta/2)$, $\theta$ is the scattering angle, $\lambda_0$ is the incident wavelength, $n$ is the refractive index, and $\tau$ is the lag time. For the studies reported here $\beta$ is close to 1.0. The polymer translational diffusion coefficient, $D(c)$, is related to $\Gamma(q)$, the characteristic relaxation frequency of the system which is taken to be the peak position of the spectra, $G(\Gamma)$, determined from eq 2 using a constrained regularization method.[48,49]

$$|g^{(1)}(q,t)| = \int G(\Gamma)e^{-\Gamma t}\,d\Gamma \quad (2)$$

$D(c)$, calculated from a linear fit of $\Gamma(q)$ vs $q^2$, is assumed to represent the translational diffusion coefficient although the condition $qR_g \ll 1.0$ is not always satisfied for the systems considered here. The dilute solution refractive index is replaced with that of the pure solvent to determine $q$. The density dependence of the refractive index is accounted for with the Lorentz−Lorenz equation which has been applied to hydrocarbon systems to 6000 bar.[50−53] The linearized Cauchy equation[54,55] is used to correct the refractive index for a $\lambda$ of 532 nm.

The concentration dependence of the mutual translational diffusion coefficient, $D(c)$, is commonly expressed as[56]

$$D(c) = D_0(1 + k_D c + ...) \quad (3a)$$

where[57]

$$k_D = 2A_2M - k_s \quad (3b)$$

Here $k_D$, the dynamic second virial coefficient that accounts for polymer−polymer and polymer−solvent interactions, is determined from the slope of $D(c)$ vs $c$, and $D_0$, the infinite dilution translational diffusion coefficient, is determined from the zero concentration intercept.[58] The change in polymer concentration with pressure is determined using solvent density data assuming the solution density equals that of pure solvent. A polymer hydrodynamic radius, $R_H$, is calculated from the Stokes−Einstein equation, $R_H = kT/6\pi\eta D_0$, where $\eta$ is the solvent viscosity. The effect of pressure on $\eta$ is determined using literature data available to moderate pressures[46] that are extrapolated to higher densities using residual viscosity and solvent density data from the literature.[40,59−61] Details on this extrapolation method are provided in the Appendix.

Figure 6 shows excellent agreement between $D_0$ for PS in toluene obtained in this study and available literature data.[22,62] $D_0$ values are corrected for the effect of molecular weight using $D_0 \propto M_w^{-0.55}$ for PS in toluene.[62−65] Note that the data of Freeman et al. differ systematically from the results presented here due to a +5% error in $D_0$ originating from detector afterpulsing[62] not encountered with the ALV system used in the present study. The values of $k_D$ and $R_H$ measured in the present study are independent of pressure and are also in excellent agreement with the data of Roots and Nystrom[22] assuming $k_D \propto M_w^{0.75}$and $R_H \propto M_w^{0.55}$ for PS in toluene.[63,64] These observations on the invariance of $R_H$ with pressure in a liquid solvent also agree with previous measurements of the intrinsic viscosity of several polymer solutions at high pressures.[66]

DLS data for the $PEB_{10}$−alkane mixtures are obtained at ~3−5 bar above the phase boundary of each binary mixture to ensure solution clarity and at much higher pressures well into the one-phase region. Figure 7 shows the effect of concentration on the mutual translational diffusion coefficient, $D(c)$, for $PEB_{10}$ in ethane, propane, butane, and pentane at 130 °C and pressures close to the phase boundary and well into the single-phase region. Straight line fits of the data suggest that eq 3a can be truncated after the linear term to obtain reliable information on $k_D$ from the slope of the line and $D_0$ from the intercept of the line at zero concentration at each pressure. Figure 8 shows the variation of $D_0$ as the system pressure is isothermally increased from the phase boundary to well into the one-phase region. The four $D_0$ curves are similar in shape, and the magnitude of $D_0$ decreases as the molecular weight of the alkane increases. Note, however, that the values of $D_0$ in Figure 8 are approximately 1 order of magnitude greater than those typically found for a polymer dissolved in a dense liquid solvent (e.g., see Figure 6) even though the alkane solvents used in this study have densities of at least ~0.5 g/cm$^3$. Figure 9 shows that $D_0$ does correlate well with "methyl" molar density which is the solvent molar density multiplied by the number of $CH_3$ + $CH_2$ groups in the solvent. The

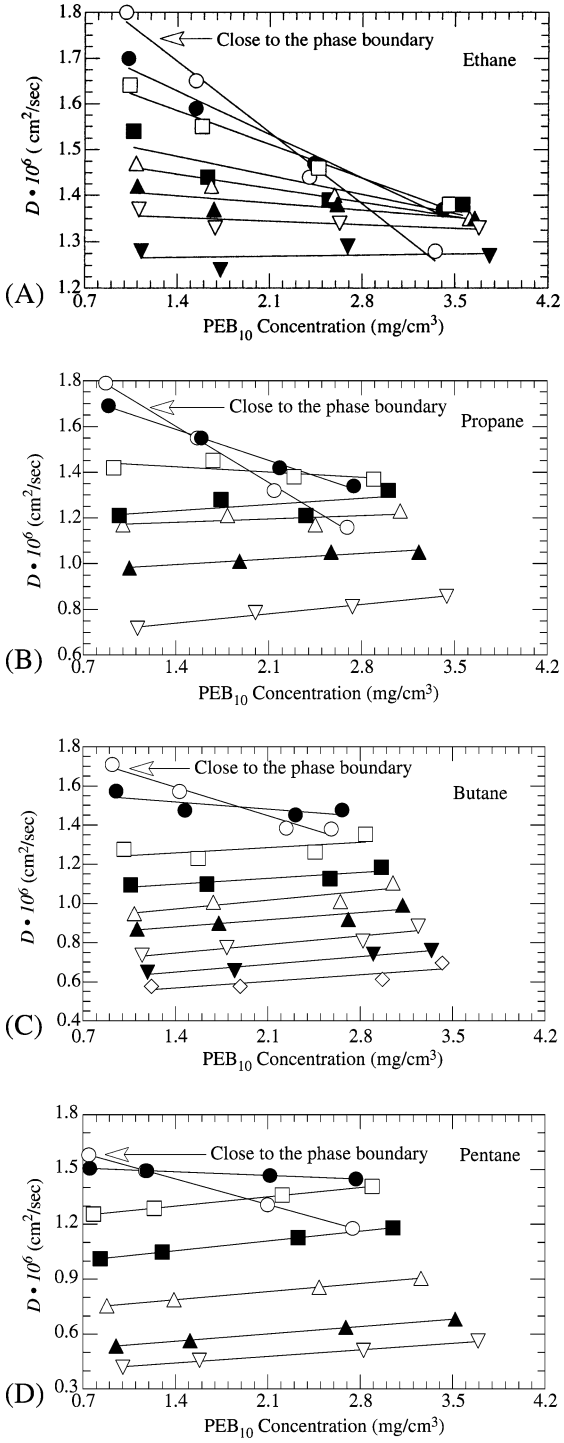


**Figure 7.** Impact of proximity to phase transition on the mutual translational diffusion coefficient, $D(c)$, for $PEB_{10}$ in ethane (A), propane (B), butane (C), and pentane (D). In (A) and (D) not all of the experimental pressures are shown to avoid cluttering the plot. (A) Open circles, 1150 bar; filled circles, 1240 bar; open square, 1310 bar; filled square, 1484 bar; open triangle, 1585 bar; filled triangle, 1650 bar; open inverted triangle, 1742 bar; filled inverted triangle, 1895 bar. (B) Open circles, 470 bar; filled circles, 520 bar; open square, 690 bar; filled square, 860 bar; open triangle, 1030 bar; filled triangle, 1380 bar; open inverted triangle, 2070 bar. (C) Open circles, 200 bar; filled circles, 275 bar; open square, 480 bar; filled square, 690 bar; open triangle, 860 bar; filled triangle, 1030 bar; open inverted triangle, 1380 bar; filled inverted triangle, 1725 bar; open diamond, 2070 bar. (D) Open circles, 50 bar; filled circles, 70 bar; open square, 170 bar; filled square, 345 bar; open triangle, 690 bar; filled triangle, 1380 bar; open inverted triangle, 2070 bar.

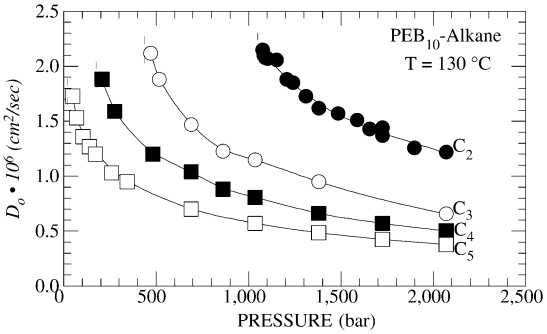


**Figure 8.** Variation of $D_0$ as a function of pressure for $PEB_{10}$ in pentane (□), butane (■), propane (○), and ethane (●). The dashed line at the start of each curve denotes the phase boundary.

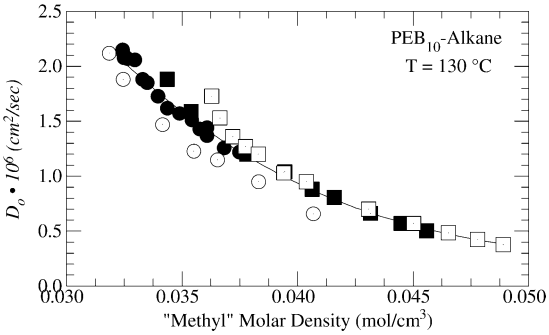


**Figure 9.** Variation of $D_0$ as a function of solvent "methyl" molar density for $PEB_{10}$ in pentane (□), butane (■), propane (○), and ethane (●). "Methyl" molar density is equal to the solvent molar density multiplied by the number of $CH_3$ and $CH_2$ groups in the alkane.

straightforward correlation shown in Figure 9 suggests that nonpolar, dispersion forces, which scale with molar mass, are likely the major contributor to the behavior of the diffusion coefficient in the one-phase region. While finer differentiation between the energetics of a $CH_3$ and a $CH_2$ group may not be warranted due to the scatter in the data, the observation that the phase boundaries occur at increasing methyl molar density for increasing solvent size may be an indication of such an influence. Unfortunately, higher simple alkanes were not considered because of insufficient scattering contrast between the polymer and the higher alkane solvents ($\geq C_6$). Figure 10 shows that as the alkane solvent size increases, decreasing $D_0$ values are not entirely accounted for by viscosity increases. Therefore, the Stokes–Einstein equation suggests $R_H$ must be changing in these solvents as the pressure is changed, assuming the Stokes–Einstein equation is valid. This behavior is not observed for the polystyrene–toluene system[62] where pressure-induced viscosity changes account for essentially the entire concurrent change in $D_0$.

As previously mentioned, Figure 7 shows that the apparent diffusion coefficient vs polymer concentration can be reliably fit with a straight line suggesting that eq 3 can be truncated after the linear term to obtain reliable information on $k_D$ from the slope of each isobar. Note that the isobars in Figure 7 exhibit negative slopes at pressures close to the system boundaries and are less negative as the pressure increases, and eventually the slopes become slightly positive at very high pressures. Similar pressure-induced changes in the sign of $k_D$, while operating in the single-phase region and close to the phase boundary, have also been observed for aqueous poly(*N*-vinyl-2-pyrrolidone) (PVP) solutions.[67] How-

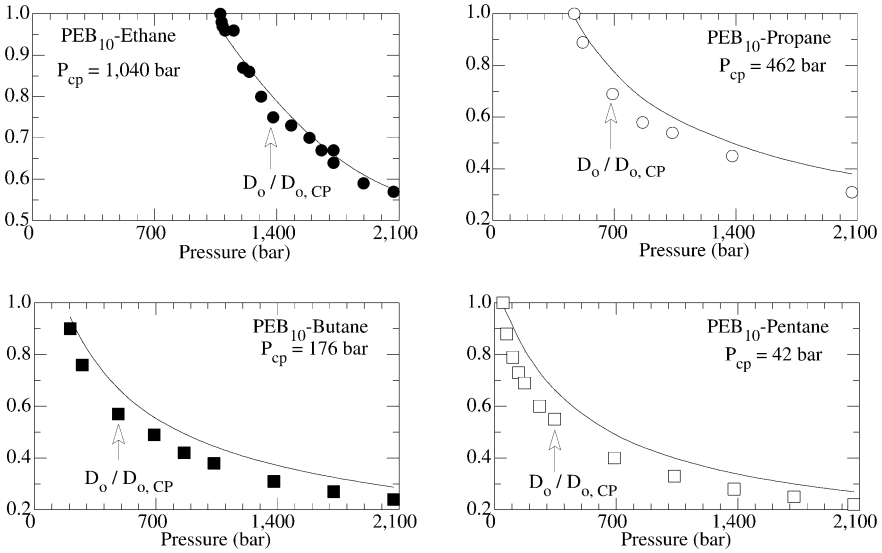


**Figure 10.** Impact of solvent viscosity, $\eta_{CP}/\eta$ (lines), on the translational diffusion coefficient, $D_0/D_{0,CP}$ (symbols), at 130 °C for the $PEB_{10}$−alkane mixtures. The cloud-point pressure, $P_{CP}$, is given in each graph; the subscript CP represents the value at the cloud point.

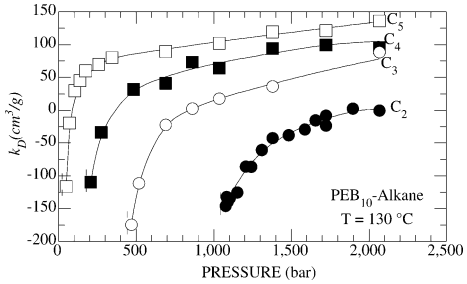


**Figure 11.** Variation of $k_D$ as a function of pressure for $PEB_{10}$ in pentane (□), butane (■), propane (○), and ethane (●). The dashed line at the start of each curve denotes the phase boundary.

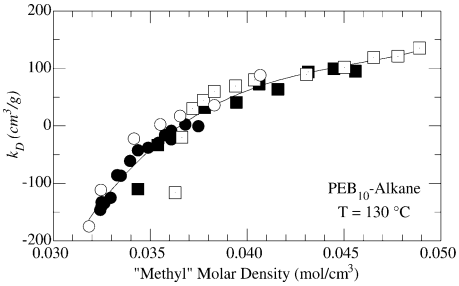


**Figure 12.** Variation of $k_D$ as a function of "methyl" molar density for $PEB_{10}$ in pentane (□), butane (■), propane (○), and ethane (●). "Methyl" molar density is equal to the solvent molar density multiplied by the number of $CH_3$ and $CH_2$ groups in the alkane.

ever, the change in the behavior of $k_D$ for the aqueous PVP solutions is related to the pressure-induced reduction in the amount of hydrogen bonding between the pyrrolidone group and water whereas the change in the behavior of $k_D$ for the $PEB_{10}$−alkane systems is related to pressure-induced (i.e., density-induced) changes in the strength of van der Waals dispersion-type interactions. Figure 11 shows the variation of $k_D$ as a function of pressure in the single-phase region. For pentane, $k_D$ increases rapidly in value from −120 to 60 $cm^3/g$ as the pressure is increased slightly above the phase transition pressure of 50 bar and then $k_D$ increases much slower with further pressure increases. The rate of increase of $k_D$ for butane is less rapid, and it takes a higher pressure before the value of $k_D$ increases above zero and then exhibits behavior that is similar to that observed for pentane. Likewise, the rate of increase of $k_D$ for propane is lower yet than that of butane although once again at high enough pressures $k_D$ reaches essentially the same values as those of butane and pentane. However, note that $k_D$ for ethane never quite becomes positive even though the system pressure exceeds 2100 bar, and the increase in $k_D$ with increasing pressure is quite sluggish. The characteristics of $k_D$ shown in Figure 11 quite clearly highlight the differences in solvent quality between compressed liquid pentane and supercritical fluid ethane. The $k_D$ curves collapse to a single curve when plotted against "methyl" molar density as defined previously (see Figure 12). Apparently, $k_D$ is dominated by the change in solvent quality which is expected to be fixed by dispersion forces as manifested in the methyl molar density.

The systems considered here are highly compressible solutions which demands that the any potential role played by solution compressibility be taken into account when interpreting the behavior of $k_D$. Schurr and coworkers[68] directly account for the concentration dependence of the mutual diffusion coefficient, $D(c)$, due to solution isothermal compressibility, $\kappa_T = -(1/V)(\partial V/\partial P)_T$, which can be shown to lead to the following expression for the dynamic second virial coefficient.

$$k_D = 2A_2M - k_s + \frac{RT\kappa_T}{M} \tag{4}$$

where $M$ is the polymer molecular weight and $k_s$ is the polymer friction coefficient. At the concentrations considered here, the solution isothermal compressibility is essentially the solvent isothermal compressibility that can be determined from the density data given in Figure 5. For comparison with previous work it is more convenient to consider the polymer volume fraction dependence of the mutual diffusion coefficient

$$D(\phi) = D_0(1 + k_D{}^{\phi}\phi + ...) \tag{5}$$

where

$$k_D{}^{\phi} = k_D \frac{M}{N_A V_H} \quad (6)$$

Here $V_H$ is an equivalent hydrodynamic hard sphere volume defined by the hydrodynamic radius $R_H$. It should be noted that the compressibility term is $\sim O(10^{-6})$, indicating that $k_D$ is essentially fixed by the thermodynamic $A_2$ and hydrodynamic $k_s$ terms.

To proceed with a discussion of $k_D{}^{\phi}$, the behavior of $R_H$ must be considered. Figure 13 shows the impact of solvent quality and proximity to the phase boundary on $R_H$ determined from the infinite dilution diffusion coefficient for the $PEB_{10}$−alkane mixtures considered in this study. Within experimental error $R_H$ appears to overlap for propane, butane, and pentane at a value of ~17 nm at the phase boundary, and then $R_H$ increases rapidly by ~12% to ~19 nm after the pressure is increased by ~100 bar. Evidently, propane, butane, and pentane switch from marginal to near theta solvents near the phase boundary to relatively good solvents at pressures just slightly removed from the phase boundary. However, the $R_H$ in ethane is relatively flat regardless of pressure, and it never exceeds ~13.5 nm, which is 30% smaller than $R_H$ in the other alkane solvents. Ethane is a poor solvent that does not have the strength to swell $PEB_{10}$ to any great extent even though the data in Figure 5 show that the density of ethane is similar to the density for the other alkane solvents especially at the respective cloud points. Therefore, unlike the infinite dilution diffusion coefficients and dynamic second virial coefficients, the hydrodynamic radius values do not scale with the "methyl" molar density of each solvent.

An examination of $k_D{}^{\phi}$ facilitates comparison with previous investigations of polymer diffusion in dilute solutions. Measured hydrodynamic radii are used to convert the measured $k_D$ to $k_D{}^{\phi}$ as defined in eq 6, and these values are presented in Figure 14 as a function of solvent "methyl" density. Although these data are more noisy than the conventional $k_D$ values presented in Figure 12, this is primarily a result of the noisy propane $R_H$ values which lead to similarly noisy propane $k_D{}^{\phi}$ values. Cotts and Selser have previously reported results for poly(α-methylstyrene) of nine different molecular weights dissolved in conventional liquid solvents ranging in quality from sub-$\theta$ to good.[58] The results observed here are very consistent with their findings. Supercritical ethane is a poor solvent and exhibits distinctly sub-$\theta$ behavior near the phase boundary, reaching only marginal quality at the highest pressures considered. Propane, butane, and pentane range in quality from near theta ($k_D{}^{\phi} = -2$)[58] to marginal (albeit better quality than ever reached for ethane) but never reaching the limit one would expect for the case of good solvents ($k_D{}^{\phi} \cong 2$).[58] Although it is not readily apparent why ethane is able to solubilize $PEB_{10}$ coils at sub-$\theta$ conditions while the other solvents fail to do so, one possible explanation may be that supercritical ethane supports fairly large length scale density fluctuations that enhance its ability to solubilize the polymer.

## Conclusions

The high-pressure DLS data presented here provide insight into the response of nonpolar $PEB_{10}$ chains to a wide variation in chemical potential environment provided by nonpolar supercritical, near critical, and compressed liquid solvents from the same chemical family. The macroscopic phase behavior for the $PEB_{10}$−alkane systems shows a nonmonotonic increase in solvent power with an increase in alkane chain length which is not unexpected.[45] The DLS data show that the polymer translational diffusion coefficient at infinite dilution, $D_0$, decreases as the alkane chain length increases. The variation of $D_0$ for propane, butane, and pentane is *not* inversely proportional with solvent viscosity even though all three solvents have very similar mass densities in the respective single-phase regions. However, the $D_0$ curves for all four alkane systems superpose if plotted against "methyl" molar density, suggesting that nonpolar, dispersion forces are likely the major contributor to the behavior of the diffusion coefficient in the one-phase region.

For propane, butane, and pentane, $k_D$, which represents a balance between thermodynamic interactions and hydrodynamic forces, starts at low negative values at conditions near the phase boundaries, increases rapidly to positive values within ~100−200 bar of the phase boundaries, and appears to slowly approach a constant value at very high pressures. However, $k_D$ for ethane, which also starts at negative values near the phase boundary, increases at a much slower rate than observed for the other alkane solvents and barely becomes greater than zero regardless of the pressure. It is apparent that ethane is a very weak solvent compared to the other alkanes even though the densities are very close to one another for all four alkanes in their respective $PEB_{10}$−alkane, single-phase regions. Also, $k_D$ values for all four $PEB_{10}$−alkane systems collapse to a single master curve when plotted against "methyl" molar density, suggesting $k_D$ variations are dominated by thermodynamic interactions rather than hydrodynamic forces. Further examination via the $k_D{}^{\phi}$ values

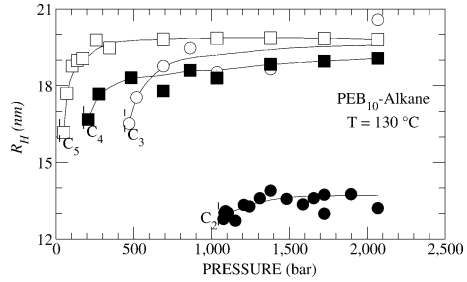


**Figure 13.** Impact of solvent quality and proximity to the phase boundary on the hydrodynamic radius, $R_H$, for $PEB_{10}$−alkane mixtures: pentane (□), butane (■), propane (○), and ethane (●). The dashed line at the start of each curve denotes the phase boundary.

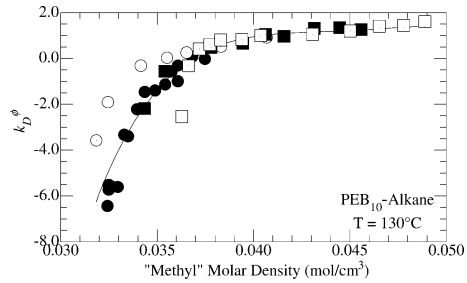


**Figure 14.** Variation of the volume fraction based dynamic second virial coefficient, $k_D{}^{\phi}$, as a function of "methyl" molar density for $PEB_{10}$ in pentane (□), butane (■), propane (○), and ethane (●). "Methyl" molar density is equal to the solvent molar density multiplied by the number of $CH_3$ and $CH_2$ groups in the alkane.

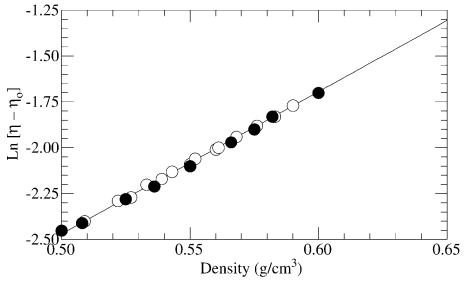


**Figure 15.** Comparison of butane viscosity from Vargaftik[46] (open circles) and Dolan et al.[59] (filled circles). The line is a fit of the data used to extrapolate viscosity data up to a butane density of 0.68 g/cm$^3$, which corresponds to the highest pressure for the DLS experiment at 130 °C.

indicates that supercritical ethane is a very poor solvent in comparison with the others.

This variation in solvent quality is also evident when comparing the behavior of $R_H$ for all four systems. $R_H$ starts low and within ~100−200 bar of the phase boundary quickly rises to a higher value which, within experimental error, is essentially the same for propane, butane, and pentane. However, $R_H$ for ethane is ~30% lower in value than the $R_H$ for the other systems, again suggesting that ethane is a poor quality solvent even 1000 bar into the single-phase region.

This coupled phase behavior−DLS study complements a previously reported SANS study of $PEB_{10}$ in supercritical ethane and in compressed liquid pentane.[35] However, in that earlier SANS study the radius of gyration, $R_g$, did not decrease as the phase boundary was approached. As noted recently by DiNoia and co-workers, the SANS data for the $PEB_{10}$−ethane and $PEB_{10}$−pentane systems were obtained with partially deuterated $PEB_{10}$ which makes it difficult to resolve unequivocally the behavior of $R_g$ as a function of pressure.[73] In addition, DiNoia and co-workers report on a technique for SANS measurements of polymer−SCF mixtures at high pressures that provides more reliable SANS data compared to the technique used in our previous study.[73] Hence, SANS experiments are currently in progress with fully deuterated $PEB_{10}$ and with the new experimental apparatus to ascertain whether $R_g$ mimics the behavior of $R_H$ as the system boundary is approached.

**Acknowledgment.** M.A.M. and J.v.Z. acknowledge the National Science Foundation (NSF) for partial support of this project under Grant CTS-9729720. Acknowledgment is made by MAM to the donors of the American Chemical Society Petroleum Research Fund for partial support of this research.

## Appendix

It was necessary to extrapolate available alkane viscosity data[46] to the high pressures used in this study. Dolan et al.[59] describe the extrapolation method, attributable to Thodos and co-workers,[69,70] which is presented here for the butane system. Dolan et al.[59] show that butane viscosity data at temperatures from 37.8 to 171 °C and pressures to 690 bar collapse to a single curve if plotted as residual viscosity, $\eta(T, P) - \eta_0(T, P = 1 \text{ atm})$, vs density. In the present DLS study this residual viscosity−density technique was used to extrapolate available viscosity data for ethane[46,71] from 0.47 to 0.57 g/cm$^3$, for propane[46,60] from 0.58 to 0.60 g/cm$^3$, for butane[46,59] from 0.60 to 0.68 g/cm$^3$, and for pentane[46,72] from 0.63 to 0.71 g/cm$^3$. Figure 15 shows representative results for the extrapolation of butane viscosity data at 130 °C. Table 2 gives the parameters used in the equation to calculate alkane viscosity.

**Table 2. Parameters for the Equation $\ln[\eta(T,P) - \eta_0(T,1)] = A + B\rho_{alkane}$ (g/cm$^3$) Used To Calculate the Viscosity of the Alkanes**

| alkane | *A* | *B* | $\eta$ (130 °C, 1 atm) |
|---|---|---|---|
| ethane | −5.556 | 6.145 | 0.012 |
| propane | −6.388 | 8.080 | 0.011 |
| butane | −6.348 | 7.757 | 0.010 |
| pentane | −6.455 | 7.847 | 0.009 |

## References and Notes

(1) Chu, B.; Lin, Y. H.; Dinapoli, A.; Nose, T.; Kuwahara, N. *Ferroelectrics* **1980**, *30*, 255−266.
(2) Chu, B. In *Scattering Techniques Applied to Supramolecular and Nonequilibrium Systems*; Chen, S.-H., Chu, B., Nossal, R., Eds.; Plenum Press: New York, 1981; Vol. 73, pp 231−264.
(3) Chu, B. *J. Polym. Sci., Polym. Symp.* **1985**, *73*, 137−155.
(4) Chu, B.; Wang, Z. *Macromolecules* **1989**, *22*, 371−374.
(5) Chu, B.; Wang, Z.; Yu, J. *Macromolecules* **1991**, *24*, 6832−6838.
(6) Chu, B. *J. Polym. Sci., Part B: Polym. Phys.* **1993**, *31*, 2019−2026.
(7) Cummins, H. Z.; Pike, E. R. *Photon Correlation and Light Beating Spectroscopy*; Plenum Press: New York, 1973.
(8) Pecora, R. In *Scattering Techniques Applied to Supramolecular and Nonequilibrium Systems*; Chen, S.-H., Chu, B., Nossal, R., Eds.; Plenum Press: New York, 1981; Vol. 73, pp 161−172.
(9) Pecora, R. In *Dynamic Light Scattering. Applications of Photon Correlation Spectroscopy*; Pecora, R., Ed.; Plenum Press: New York, 1985; pp 1−6.
(10) Gaeckle, D.; Patterson, D. *Macromolecules* **1972**, *5*, 136−141.
(11) Freeman, B. D. In *Chemical Engineering*; University of California: Berkeley, 1988.
(12) Moki, Y.; Takenaka, T. *Sci. Eng. Rev. Doshisha Univ.* **1998**, *39*, 15−20.
(13) Claesson, S.; Malmrud, S.; Lundgren, B. *Trans. Faraday Soc.* **1970**, *66*, 3048−3052.
(14) Richards, C. J.; Fisch, M. R. *Rev. Sci. Instrum.* **1994**, *65*, 335−338.
(15) Szydlowski, J.; Rebelo, L. P. N.; Wilczura, H.; Dadmun, M.; Melnichenko, Y. B.; Wignall, G. D.; van Hook, W. A. *Phys. B* **1998**, *241−243*, 1035−1037.
(16) Szydlowski, J.; Rebelo, L. P. N.; Wilczura, H.; Dadmun, M.; Melnichenko, Y. B.; Wignall, G. D.; van Hook, W. A. *Fluid Phase Equilib.* **1998**, *150−151*, 687−694.
(17) Buhler, E.; Dobrynin, A. V.; DeSimone, J. M.; Rubenstein, M. *Macromolecules* **1998**, *31*, 7347−7355.
(18) van Hook, W. A.; Wilczura, H.; Imre, A.; Rebelo, L. P. N.; Melnichenko, Y. B. *Macromolecules* **1999**, *32*, 7312−7318.
(19) Van Hook, W. A.; Wilczura, H.; Rebelo, L. P. N. *Macromolecules* **1999**, *32*, 7299−7311.
(20) McDonald, C. J.; Claesson, S. *Chem. Scr.* **1973**, *4*, 155−162.
(21) McDonald, C. J.; Claesson, S. *Chem. Scr.* **1976**, *9*, 36−46.
(22) Roots, J.; Nystrom, B. *Macromolecules* **1982**, *15*, 553−556.
(23) Zhou, S.; Chu, B.; Dhadwal, H. S. *Rev. Sci. Instrum.* **1998**, *69*, 1−6.
(24) Koga, T.; Zhou, S. Q.; Chu, B. *Appl. Opt.* **2001**, *40*, 4170−4178.
(25) Lechner, M. D.; Schulz, G. V. *J. Colloid Interface Sci.* **1972**, *39*, 469−471.
(26) Lechner, M. D.; Schulz, G. V.; Wolf, B. A. *J. Colloid Interface Sci.* **1972**, *39*, 462−468.
(27) Lechner, M. D. *Ber. Bunsen.-Ges.* **1977**, *10*, 992−995.
(28) Jeremic, K.; Ilic, L.; Jovanovic, S.; Lechner, M. D. *Eur. Polym. J.* **1989**, *25*, 281−284.
(29) Stankovic, R. I.; Jovanovic, S.; Ilic, L.; Nordmeier, E.; Lechner, M. D. *Polymer* **1991**, *32*, 235−240.
(30) Leimkuhler, M.; Goldbeck, A.; Lechner, M. D.; Witz, J. *J. Mol. Biol.* **2000**, *296*, 1295−1305.
(31) Nordmeier, E.; Lechner, M. D. *Macromolecules* **1991**, *24*, 2529−2537.
(32) Szydlowski, J.; van Hook, W. A. *Macromolecules* **1998**, *31*, 3255−3265.

(33) Szydlowski, J.; van Hook, W. A. *Macromolecules* **1998**, *31*, 3266−3274.
(34) Moses, C. L.; van Hook, W. A. *J. Polym. Sci., Part B: Polym. Phys.* **2003**, *41*, 3070−3076.
(35) DiNoia, T. P.; Kirby, C. F.; van Zanten, J. H.; McHugh, M. A. *Macromolecules* **2000**, *33*, 6321−6329.
(36) Miller, K. J.; Savchik, J. A. *J. Am. Chem. Soc.* **1979**, *101*, 7206−7213.
(37) Reid, R. C.; Prausnitz, J. M.; Poling, B. E. *The Properties of Gases and Liquids*, 4th ed.; McGraw-Hill: New York, 1987.
(38) Diguet, R.; Deul, R.; Franck, E. U. *Ber. Bunsen-Ges. Phys. Chem.* **1985**, *89*, 800−804.
(39) Sen, Y. L.; Kiran, E. *J. Supercrit. Fluids* **1990**, *3*, 91−99.
(40) Byun, H. S.; DiNoia, T. P.; McHugh, M. A. *J. Chem. Eng. Data* **2000**, *45*, 810−814.
(41) Rachapudy, H.; Smith, G. G.; Raju, V. R.; Graessley, W. W. *J. Polym. Sci., Part B: Polym. Phys.* **1979**, *17*, 1211−1222.
(42) Kirgas, T. M.; Carella, J. M.; Struglinski, M. J.; Crist, B.; Graessley, W. W. *J. Polym. Sci., Part B: Polym. Phys.* **1985**, *23*, 509.
(43) Balsara, N. P.; Fetters, L. J.; Hadjichristidis, N.; Lohse, D. J.; Han, C. C.; Graessley, W. W.; Krishnamoorti, R. *Macromolecules* **1992**, *25*, 6137−6147.
(44) Fetters, L. J.; Graessley, W. W.; Krishnamoorti, R.; Lohse, D. J. *Macromolecules* **1997**, *30*, 4973−4977.
(45) Kirby, C. F.; McHugh, M. A. *Chem. Rev.* **1999**, *99*, 565−602.
(46) Vargaftik, N. B. *Tables on the Thermophysical Properties of Liquids and Gases: In Normal and Dissociated States*, 2nd ed.; Hemisphere Publishing Corp.: Washington, DC, 1975.
(47) Sen, Y. L.; Kiran, E. *Int. J. Thermophys.* **1992**, *13*, 411−412.
(48) Provenecher, S. W. *Comput. Phys. Commun.* **1982**, *27*, 213−227.
(49) Provenecher, S. W. *Comput. Phys. Commun.* **1982**, *27*, 229−242.
(50) Hadrich, J. *Appl. Phys.* **1975**, *7*, 209−213.
(51) Vedam, K.; Limsuwan, P. *J. Chem. Phys.* **1978**, *69*, 4772−4778.
(52) Achtermann, H. J.; Magnus, G.; Bose, T. K. *J. Chem. Phys.* **1991**, *94*, 5669−5684.
(53) Conway, S. E. In *Chemical Engineering*; Johns Hopkins University: Baltimore, MD, 2001.
(54) Johnson, B. L.; Smith, J. In *Light Scattering from Polymer Solutions*; Huglin, M. B., Ed.; Academic Press: New York, 1972; pp 27−39.
(55) Born, M.; Wolf, E. *Principles of Optics: Electromagnetic Theory of Propagation, Interference and Diffraction of Light*, 7th ed.; Cambridge University Press: New York, 1999.
(56) Vink, H. *Faraday Trans.* **1985**, *81*, 1725.
(57) Tsunashima, Y.; Hashimoto, T.; Nakano, T. *Macromolecules* **1996**, *29*, 3475−3484.
(58) Cotts, P. M.; Selser, J. C. *Macromolecules* **1990**, *23*, 2050−2057.
(59) Dolan, J. P.; Starling, K. E.; Lee, A. L.; Eakin, B. E.; Ellington, R. T. *J. Chem. Eng. Data* **1963**, *8*, 396−399.
(60) Starling, K. E.; Eakin, B. E.; Ellington, R. T. *AIChE J.* **1960**, *6*, 438−442.
(61) Kashiwagi, H.; Makita, T. *Int. J. Thermophys.* **1982**, *3*, 289−305.
(62) Freeman, B. D.; Soane, D. S.; Denn, M. M. *Macromolecules* **1990**, *23*, 245−251.
(63) Berry, G. C. *J. Chem. Phys.* **1966**, *44*, 4550−4564.
(64) Wiltzius, P.; Haller, H. R.; Cannell, D. S. *Phys. Rev. Lett.* **1984**, *53*, 834−837.
(65) Will, S.; Leipertz, A. *Appl. Opt.* **1993**, *32*, 3813−3821.
(66) Cook, R. L.; King, H. E., Jr.; Peiffer, D. G. *Macromolecules* **1992**, *25*, 2928−2934.
(67) Sun, T.; King, H. E., Jr. *Phys. Rev. E* **1996**, *54*, 2696−2703.
(68) Allison, S. A.; Chang, E. L.; Schurr, J. M. *Chem. Phys.* **1979**, *38*, 29−41.
(69) Brebach, W. J.; Thodos, G. *AIChE J.* **1958**, *4*, 1095−1100.
(70) Shimotake, H.; Thodos, G. *AIChE J.* **1958**, *4*, 257−262.
(71) Eakin, B. E.; Starling, K. E.; Dolan, J. P.; Ellington, R. T. *J. Chem. Eng. Data* **1962**, *7*, 33−36.
(72) Lee, A. L.; Ellington, R. T. *J. Chem. Eng. Data* **1965**, *10*, 101−104.
(73) DiNoia, T. P.; van Zanten, J. H.; Kline, S. R.; Garach-Domech, A.; McHugh, M. A.; Wright, P. J.; Fetters, L. J. *Macromolecules* **2003**, *36*, 7372−7378.

MA0487103